Res Chem Intermed (2014) 40:1595–1605
DOI 10.1007/s11164-013-1064-9

Sonochemical synthesis of Fe–TiO_2–SiC composite for degradation of rhodamine B under solar simulator

Tae Ho Kim · Christian Gómez-Solís · Edgar Moctezuma · Soo Wohn Lee

Received: 10 September 2012 / Accepted: 15 January 2013 / Published online: 30 January 2013

Abstract Fe–TiO_2–SiC composite with photocatalytic activity has been synthesized by a low cost sonochemical process in the presence of citric acid. The addition of citric acid during the sonochemical process allows the formation of a photocatalytic coating of Fe–TiO_2 onto silicon carbide. Experimental characterization results indicate that the composite was formed over all the surface of the silicon carbide (SiC) with an anatase crystalline TiO_2 phase with iron incorporation. The incorporation of iron narrows the band gap of TiO_2 which allow the absorbtion of light with a large wavelength. The obtained Fe–TiO_2–SiC composite exhibits good enhanced photocatalytic activity for the degradation of rhodamine B under solar simulator irradiation in comparison with the commercial TiO_2–P25.

Keywords Silicon carbide · Sonochemistry · Photodegradation · Solar simulator · Rhodamine B

Introduction

One of the keys for enhancing the photoactivity of TiO_2 as a photocatalyst is to increase the mass transfer and adsorption of contaminants onto the surface of the photocatalyst. Normally, doping the TiO_2 with transitions metals [1–4], metals, and also heterojunctions with other oxides [5–8], increases the surface area, improves the transfer of photogenerated electrons prolonging charge carrier lifetime, and the

T. H. Kim · S. W. Lee (✉)
Research Center for Eco Multi-Functional Nano Materials, Sun Moon University, Galsan-ri, Tangjung-Myon, Asan Chungnam, Republic of Korea
e-mail: swlee@sunmoon.ac.kr

C. Gómez-Solís · E. Moctezuma
Facultad de Ciencias Químicas, Universidad Autónoma de San Luis Potosí, Av. Manuel Nava #6, 78290 San Luis Potosí, SLP, Mexico

ability of working under visible-light irradiation [9, 10]. Another way to increase the surface phenomena to enhance the photoactivity is to support the TiO_2 on different heterogeneous catalyst supports, e.g., light-weight materials [11], high surface materials (as activated carbons) [12–17], resistance mechanical materials (as silicon carbide) [18], and some plastic materials [19].

However, the success of these composite systems has to cope with the difficulty in controlling the TiO_2 deposition to obtain a highly dispersed coating with stability, photoactivity, and synthesis at low cost [20–23]. Some coatings are manufactured by complicated and expensive methods, like chemical vapor deposition [24], ion exchange methods [25], hydrothermal reduction methods [26], and sonochemical deposition [27–29]. Ultrasonic deposition has proved to be an effective technique for generating nanoparticles with attractive properties in a short period of reaction time [30]. The enhanced chemical effect of ultrasound is due to acoustic cavitation phenomena. The major advantage of this method, apart from its fast quenching rate and operation at ambient condition, is that it is a simple and energy efficient process [31].

Silicon carbide (SiC) has already been employed as a heterogeneous catalyst support for the oxidation and photodegradation of organic contaminants [7, 8], because SiC exhibits a low coefficient of thermal expansion, good resistance to the oxidation (formation of protective silica layer) [32], and larger surface area.

In the present work, silicon carbide (SiC) was utilized as support of Fe-doped TiO_2. Fe–TiO_2–SiC photocatalyst was prepared by the sonochemistry method. The composite has been tested as a photocatalyst for degradation of rhodamine B dye under a solar simulator.

Experimental

Fabrication of Fe–TiO_2–SiC composite

The composite was prepared using SiC (mesh 200–450; Sigma–Aldrich), titanium butoxide (97 %; Sigma–Aldrich) and Iron (III) chloride (97 %; Sigma–Aldrich) without any further purification as precursor. Fe–TiO_2–SiC was prepared from the aqueous slurry of SiC and crystallization of Fe-doped TiO_2. The sonochemical method was carried out as follows: 20 mL of ethylene glycol was heated at 60 °C in a beaker and 4 mL of titanium butoxide was added by dropping, and stirred for 10 min. The mechanical mixture of 0.3 g of citric acid, 100 mg of ferric chloride and 0.8 g of SiC particles were added slowly to the solution. Finally, the obtained suspension was sonicated at room temperature for 3 h at 20 kHz, 400 W cm^{-2} ultrasonic conditions. The resulting composite was recovered by centrifugation at 10,000 rpm for 15 min, then the composite was washed with deionizer water and then with absolute ethanol to remove unreacted reagents, and dried in a freeze-drier for 24 h. Finally, the dry powder was thermally treated at 450 °C for 2 h.

Characterization of Fe–TiO_2–SiC composite

The crystalline structure of Fe–TiO_2–SiC composite was evaluated by using an X-ray diffractometer (Rigaku 2200). The X-ray diffraction patterns were acquired

over the 2θ range from 20° to 90° at the scanning rate of 0.05° per minute. The surface morphology and particle size of the material were examined by field-emission scanning electron microscope (FE-SEM; JSM-6700F), coupled with energy dispersive spectroscopy (EDS) to determine the composition of the particles. Surface area was measured by the BET method with a Quantachrome NOVA 2000e instrument using nitrogen as adsorbate. The energy band gap (*Eg*) was determined by UV–Vis spectroscopy using a Perkin Elmer Lamda 35 spectrometer equipped with an integrating sphere. The analysis was conducted between 200 and 650 nm.

Photocatalytic experiments

Photocatalytic degradation experiments were carried out in a Petri dish reactor irradiated with solar simulator (portable solar simulator PEC-L01; Pecell) (Am 1.5G). For each experiment, 50 mL of an aqueous solution of rhodamine B (5 ppm) were placed inside the petri dish coated with 100 mg photocatalytic powder into a thin layer. The preparation of the thin layer, was achieved in Petri dish reactor, by a dispersion in absolute ethanol. The solution was sonicated for 10 min then dried for 24 h in an oven at 343 K. Samples for analysis were taken at different times to monitor the advance of the reaction using a MECASYS Optizen 2120UV Spectrophotometer. The concentration of rhodamine B in the solution was determined as a function of irradiation time using the intensity of the main absorbance band at a wavelength of 550 nm.

Results and discussion

Figure 1 shows the XRD patterns of Fe–TiO_2–SiC composite prepared by the sonochemical method and after thermal treatment at 450 °C, for TiO_2–P25 and SiC. The XRD characteristic peaks of anatase, rutile, and SiC are clearly observed. The very broad peak at 25.5 (2θ) of the Fe–TiO_2–SiC composite indicates the nanocrystallinity of Fe–TiO_2 formed on the SiC particles. The XRD patterns show the peaks for anatase and SiC. It is important to note the absence of the rutile phase, which normally appears during thermal treatment above 400 °C [33]; therefore, in this case, we assume that the soft conditions used for the synthesis of TiO_2 allow the avoidance of the transformation of the rutile phase. In addition, the absence of secondary phases indicates that there is no chemical reaction between Fe–TiO_2 and SiC during the sonochemical process and after thermal treatment at 450 °C. The effect of the Fe metal doping into TiO_2 was investigated by Luu and his coworkers [34]. Doping of Fe into TiO_2 indicated that some Fe^{3+} ions probably replace some Ti^{4+} ions in the crystal framework of TiO_2. Based on the X-ray diffraction analysis, the Fe doping influences the size of the crystallite anatase phase.

The FE-SEM images of the commercial SiC and Fe–TiO_2–SiC composite are shown in Fig. 2a, b. Figure 2a shows that the size of commercial SiC particle observed was around 50 μm with irregular morphology. Figure 2b shows that the presence of TiO_2 nanoparticles deposited on the SiC surface can be observed; TiO_2 particles were coated, homogeneously in the SiC surface with a size lower than 100 nm.

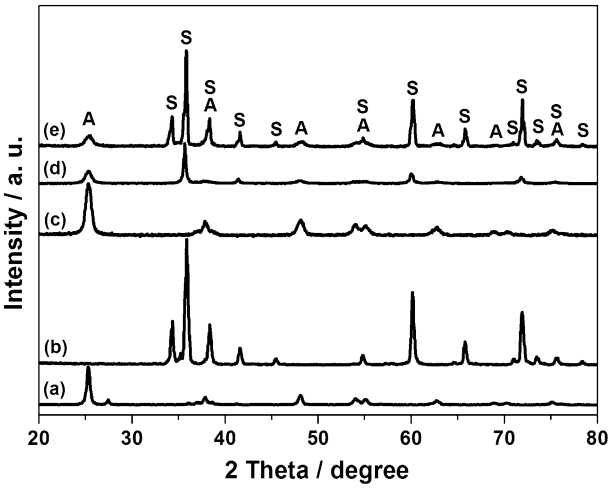

Fig. 1 XRD patterns of photocatalysts **a** TiO_2–P25, **b** SiC, **c** Fe–TiO_2, **d** TiO_2–SiC, and **e** Fe–TiO_2–SiC composite

Furthermore, it is observed that, due to the physical interaction of TiO_2 nanoparticles, the TiO_2–Fe are agglomerated homogeneously over the entire SiC surface. However, some small amounts of Fe and TiO_2 nanoparticles were also overgrown to form bundles, which possibly are not well homogenized during sonochemical synthesis.

In the sonochemical synthesis, it is well known that loaded nanoparticles are incorporated into supports [31]. Figure 3 shows, from the results of the SEM imaging and EDS elemental mapping, that the presence of 0.38 wt% of Fe on/in the particles of SiC were highly and uniformly dispersed. In the mapping, one can observe that the nanoparticles of TiO_2 were dispersed on the particles of SiC, as well as the Fe nanoparticles. This confirms that the sonochemistry technique provides homogeneous dispersion of Fe–TiO_2 over SiC particles.

The diffuse reflectance UV–vis spectra of the TiO_2–P25, Fe–TiO_2, TiO_2–SiC, Fe–TiO_2–SiC composite, and SiC are shown in Fig. 4. All the prepared samples were red-shifted and extended absorption in the visible-light region compared with TiO_2–P25. Wantala et al. [35] reported the diffuse reflectance UV–Vis spectra absorption bands of Fe–TiO_2 catalysts at 412 and 500 nm. The band at 412 nm was assigned to the charge transfer of Fe^{3+} to the TiO_2 conduction band according to the energy level of 3d electrons. The apparent valence state of Fe-doped TiO_2 was predominantly found to be 3+. Another band at 500 nm is attributed to d–d transition of charge transfer of Fe ions as:

$$Fe^{3+} + Ti^{3+} \rightarrow Fe^{2+} + Ti^{4+} \quad (1)$$

The TiO_2–SiC and Fe–TiO_2–SiC composite shows an absorption edge at 400 nm in Fig. 4. The absorption edges shift toward longer wavelengths for the Fe–TiO_2–SiC composite. The loading of Fe onto TiO_2–SiC can significantly improve the spectral absorption. It can be seen that the band gap energies (*Eg*) found for the supports are higher than those obtained with the Fe–TiO_2 and TiO_2–SiC in Table 1.

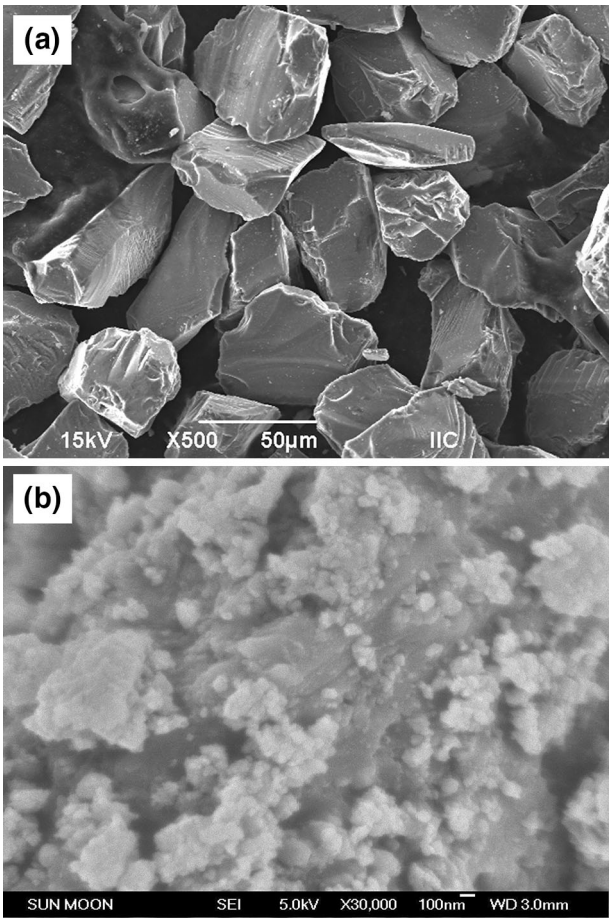

Fig. 2 FE-SEM micrographs of **a** SiC and **b** Fe–TiO_2–SiC composite after thermal treatment at 450 °C for 2 h

The absorption coefficient α can be calculated according to the Kubelka–Munk method based on the diffuse reflectance spectra [36–38], and the estimated band gap energies for the photocatalysts are 3.0 3.2, 2.9, 2.7, and 2.4 eV for the SiC, TiO2–P25, Fe–TiO_2, TiO_2–SiC, and Fe–TiO_2–SiC composite, respectively. The reason might be that the loading of Fe and TiO_2 onto the SiC forms new energy levels between the valance band and the conduction band within the band gap of SiC and TiO_2. This could enhance the photocatalytic behavior for degradation reactions because a synergy effect in Fe–TiO_2–SiC composite could happen, as Yamashita et al. [7] mentioned in a previous work.

The specific surface areas of the produced photocatalytic powders are listed in Table 1. For the SiC and TiO_2–P25 reference materials, the BET surface areas are 19 and 56 $m^2\ g^{-1}$, respectively; for the Fe–TiO_2, TiO_2–SiC, and Fe–TiO_2–SiC composite, the BET surface areas are 66, 37, and 139 $m^2\ g^{-1}$, respectively. These

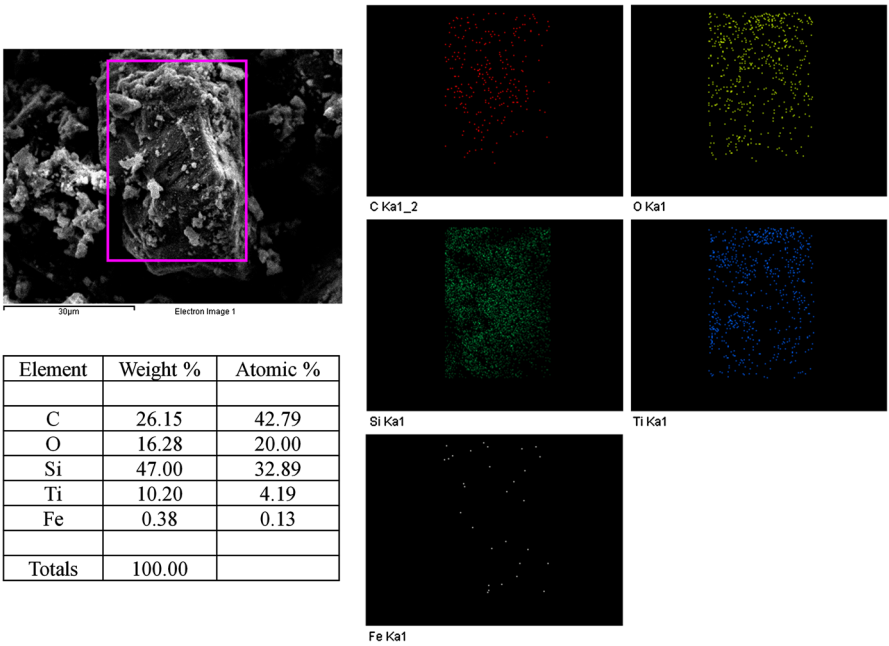

Element	Weight %	Atomic %
C	26.15	42.79
O	16.28	20.00
Si	47.00	32.89
Ti	10.20	4.19
Fe	0.38	0.13
Totals	100.00	

Fig. 3 X-ray EDS images of Fe–TiO_2–SiC composite after thermal treatment at 450 °C for 2 h

results indicate a remarkable increase in surface area with the use of Fe and TiO_2 nanoparticles on the surface of SiC.

XPS spectra of Ti 2p in Fe–TiO_2–SiC composite (Fig. 5a) reveal that the Ti $2p_{1/2}$ and Ti $2p_{2/3}$ peak positions at 464.5 and 459 eV are in good agreement with those

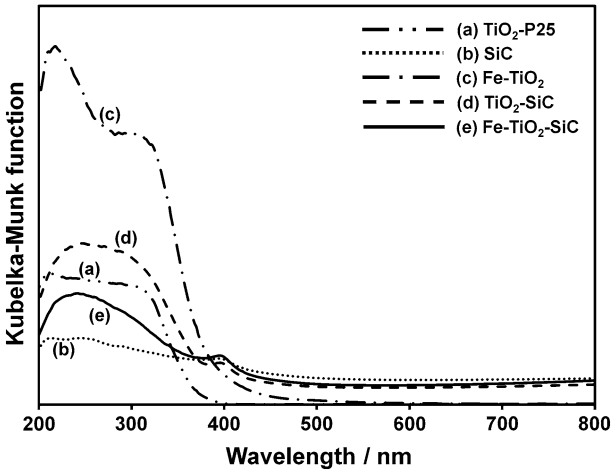

Fig. 4 Diffuse reflectance UV–vis spectra of **a** TiO_2–P25, **b** SiC, **c** Fe–TiO_2, **d** TiO_2–SiC, and **e** Fe–TiO_2–SiC composite

Table 1 Energy band gap (E_g) and specific surface area (S_{BET}) of Fe–TiO_2–SiC composite as photocatalysts

Sample	E_g (eV)	S_{BET} ($m^2\ g^{-1}$)
SiC	3.0	19
TiO_2–P25	3.2	56
Fe–TiO_2	2.9	66
TiO_2–SiC	2.7	37
Fe–TiO_2–SiC	2.4	139

observed for the Ti^{4+} species reported in previous literature [39]. Figure 5b shows the XPS spectra of Fe 2p in Fe–TiO_2–SiC composite. The Fe $2p_{1/2}$ and Fe $2p_{3/2}$ peaks at 724.3 and 710.9 eV indicate that Fe^{3+} is present on the Fe–TiO_2–SiC surface [1]. Thus, the Fe exists in common Fe^{3+} oxidation state. Since the ionic radius of Fe^{3+} (0.64 Å) and Ti^{4+} (0.68 Å) are similar, the Fe^{3+} could be incorporated into the lattice of TiO_2 to form Ti–O–Fe bond in the Fe–TiO_2 [40]. Figure 5c, d shows the XPS spectra of Si 2p and C 1 s in Fe–TiO_2–SiC composite. For crystalline SiC, the typical binding energy of C 1 s and Si 2p is 280.7 ~ 283.0 eV and 99.7 ~ 100.8 eV, respectively [41]. Two binding energy peaks of Si 2p are 100.8 and 102.9 eV, corresponding to the Si–C and Si–O bonds, respectively. Correspondingly, two binding energy peaks of C 1 s are 283.4 and 284.6 eV, corresponding to the one of C 1 s in C–Si and C–C bonds in the Fe–TiO_2–SiC composite.

The photocatalytic activities of the TiO_2–P25, SiC, Fe–TiO_2, TiO_2–SiC, and Fe–TiO_2–SiC composite were evaluated on the photocatalytic degradation of rhodamine B under solar light irradiation as a test reaction. The photocatalytic degradation of the rhodamine B as a function of time is shown in Fig. 6. The corresponding activities are reported as half-life time $t_{1/2}$ in Table 2. The lowest activities correspond to the TiO_2–P25, SiC, Fe–TiO_2, and TiO_2–SiC photocatalyst ($t_{1/2}$ of 182, 630, 126. and 110 min, respectively). However, the obtained Fe–TiO_2–SiC composite showed the highest photoactivity, $t_{1/2} = 36$ min (Table 2). The photocatalytic degradation of rhodamine B using TiO_2–P25, SiC, Fe–TiO_2, TiO_2–SiC, and Fe–TiO_2–SiC composite after 120 min in solar light irradiation reaches the percentages of 37, 11, 50, 55, and 90 %, respectively, with different behaviors (see Fig. 6). Figure 6 indicates that Fe–TiO_2–SiC composite prepared by sonochemical method is more active for the degradation of rhodamine B after 120 min of reaction, and its performance is even better than the TiO_2–P25, SiC, Fe–TiO_2, and TiO_2–SiC. The photocatalytic degradation reaction with coated samples approximately obeys pseudo-first-order kinetics, and the apparent rate constant was calculated by plotting $\ln(C_0/C)$ versus time, as shown in Fig. 7. The calculated values presented in Table 2 indicate that the Fe–TiO_2–SiC composite prepared by the sonochemical method have the highest value of the kinetic constant.

The nanoparticles of Fe–TiO_2 have been achieved by a sonochemical method. The process involves a stable coating of TiO_2–Fe on the SiC surface by hydroxyl groups that can interact with the Ti–Fe through charge transfer interaction. Hence, the Ti and Fe ions might become attached to the surface. The citric acid is used to control the size of nanoparticles and prevent big aggregation. This is because, in general, surface functionalization is needed in order to be effective for homogeneous dispersion. The ultrasonic agitation can disperse solutes homogeneously in

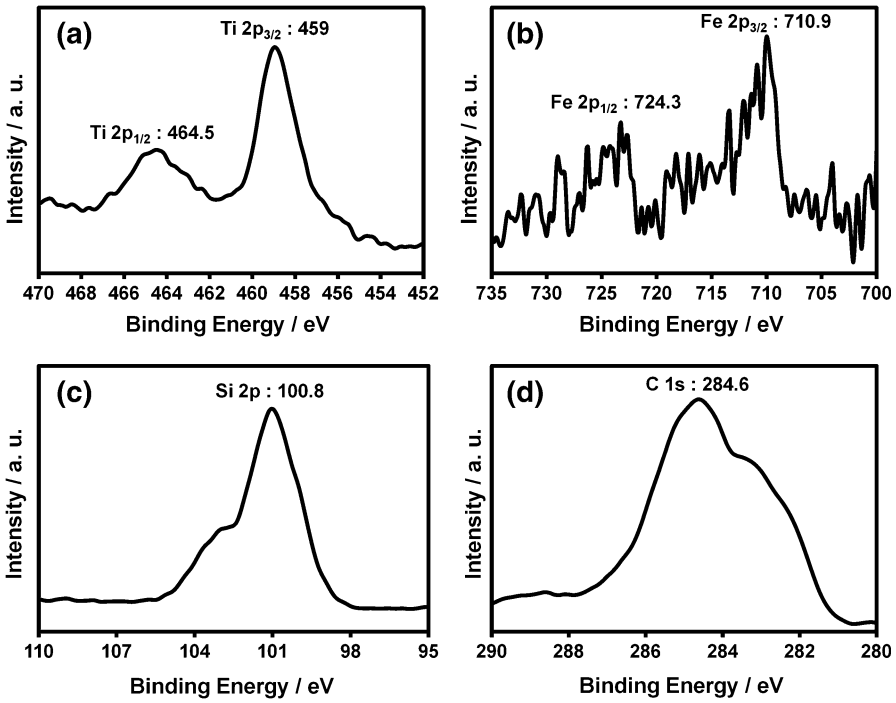

Fig. 5 XPS spectra of Fe–TiO_2–SiC composite: **a** Ti 2p, **b** Fe 2p, **c** Si 2p, and **d** C 1 s

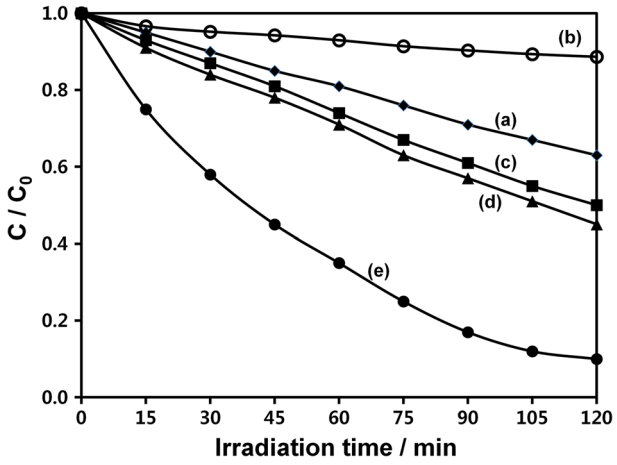

Fig. 6 Photocatalytic degradation of the rodamine B solution for different TiO_2 under solar light: **a** TiO_2–P25, **b** SiC, **c** Fe–TiO_2, **d** TiO_2–SiC, and **e** Fe–TiO_2–SiC composite

the mixture and enhance the diffusion rate of titanium butoxide to the surface of the SiC particles, which can interact with the metal cation forming Ti–O–Si bonds in the SiC surface.

Table 2 Kinetic parameters for rhodamine B dye photodegradation using Fe–TiO_2–SiC composite as photocatalysts

Sample	Degradation percentage (%)	k′ (min^{-1})	Half-life time (min)
SiC	11	0.0011	630
TiO_2–P25	37	0.0038	182
Fe–TiO_2	50	0.0055	126
TiO_2–SiC	55	0.0063	110
Fe–TiO_2–SiC	90	0.0192	36

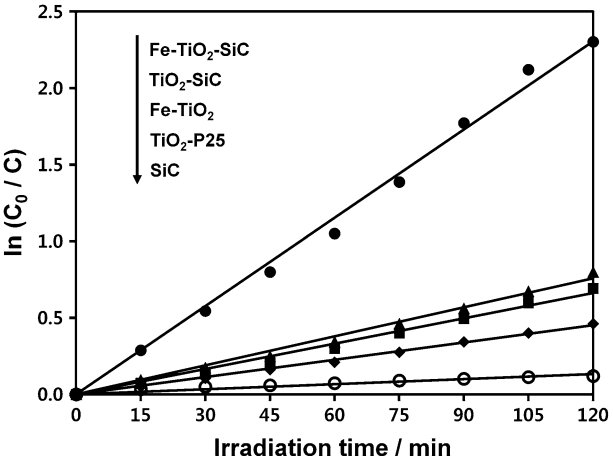

Fig. 7 Pseudo-first-order kinetics and apperent rate constant for the rodamine B degradation

Figure 8 proposes a schematic representation of transfer of photons. The photocatalytic incremental activity under a solar simulator of the material Fe–TiO_2–SiC composite compared with TiO_2–P25 is attributed to the narrow band gap. For the material Fe–TiO_2–SiC composite, the increment in activity may be due to a synergy effect between Fe–TiO_2 that can effectively absorb the light with a large wavelength and homogeneously dispersed on the SiC surface, and the sonochemical method generates enough energy to melt the contact region of two different solid particles that will behave as a heterojunction as described by Yamashita et al. [9]. The particles of SiC are partially recovered, because the ultrasonic agitation disperses solutes homogeneously in the mixture and enhances the diffusion rate of titanium butoxide and $FeCl_3$ to the surface of SiC; also SiC particles do not affect the band gap of the Fe–TiO_2. The dispersion on the surface of the titania-modified particles allows the improvement in the mass transfer with the pollutants and generates a good synergy among both, which favors their photocatlytic activity as shown in Fig. 8. It was also observed that Fe–TiO_2–SiC composite are easily separated from the reaction mixture because the heavy SiC particles settle down after the mechanical agitator of the photoreactor is turned off. Also, iron can change the oxidation states 3+ and 2+ to help the electronic transfer during the photocatalytic process [42, 43].

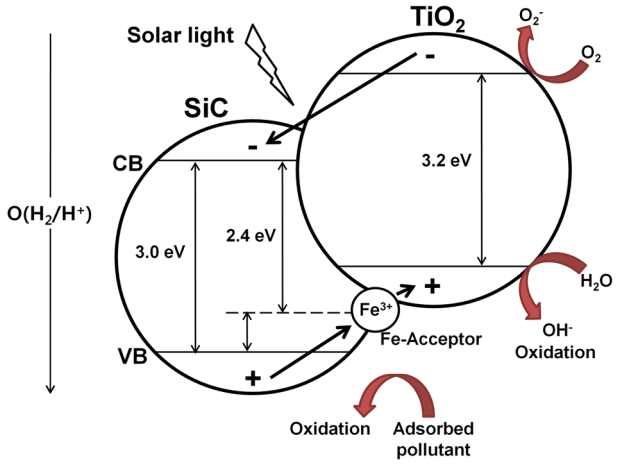

Fig. 8 A mechanism for the photocatalytic decomposition of pollutants by the coupling of an Fe–TiO_2–SiC composite

Conclusions

The results indicated that rhodamine B could be photodegradated by Fe–TiO_2–SiC composite prepared by a sonochemical method under a solar simulator. Particularly, Fe–TiO_2–SiC composite showed a higher photocatalytic activity than TiO_2–SiC, Fe–TiO_2, SiC, and commercial TiO_2–P25 powder. Photocatalytic activity is due to the well-dispersed Fe–TiO_2 nanoparticles on the surface of SiC. The composite permits more efficient mass transfer of the contaminants, and the highly dispersed TiO_2–Fe particles could absorb solar light at larger wavelengths due to the narrow band gap induced from iron incorporation.

Acknowledgment This research was supported by the GRL program through the National Research Foundation of Korea funded by the Ministry of Education, Science and Technology (20110-00339).

References

1. J.G. Yu, Q.J. Xiang, M.H. Zhou, Appl. Catal. B **90**, 595 (2009)
2. S. Yuan, R.Q. Sheng, J.L. Zhang, F. Chen, Surf. Sci. Catal. **165**, 261 (2007)
3. K. Bhattacharyya, A.K. Patra, P.U. Sastry, A.K. Tyagi, J. Alloy Comp. **482**, 256 (2009)
4. F.J. Ren, Y.H. Ling, J.Y. Feng, Appl. Surf. Sci. **256**, 3735 (2010)
5. W.Y. Choi, A. Termin, M.R. Hoffmann, J. Phys. Chem. **98**, 13669 (1994)
6. V. Keller, P. Bernhardt, F. Garin, J. Catal. **215**, 129 (2003)
7. H. Yamashita, Y. Nishida, S. Yuan, K. Mori, M. Narisawa, Y. Matsumura, T. Ohmichi, I. Katayama, Catal. Today **120**, 163 (2007)
8. N. Keller, V. Keller, F. Garin, M.J. Ledoux, Mater. Lett. **58**, 970 (2004)
9. T. Zhang, T. Oyama, S. Horikoshi, J. Zhao, N. Serpone, H. Hidaka, Appl. Catal. B **42**, 13 (2003)
10. N. San, A. Hatipoglu, G. Kocturk, Z. Cinar, J. Photochem. Photobiol. A **146**, 189 (2002)
11. S. Obregón Alfaro, V. Rodríguez-González, A.A. Zaldívar-Cadena, S.W. Lee, Catal. Today **166**, 166 (2011)
12. S. Zhang, Z. Chen, Y. Li, Q. Wang, L. Wan, Y. You, Mater. Chem. Phys. **107**, 1 (2008)
13. A.N. Oket, E. Sayinsoz, Sep. Purif. Technol. **62**, 535 (2008)

14. T. Zhang, L. Ge, X. Wang, Z. Gu, Polymer **49**, 2898 (2008)
15. S. Zhang, Z. Chen, Y. Li, Q. Wang, L. Wan, Catal. Commun. **9**, 1178 (2008)
16. K.C. Remant Bahadur, C.K. Kim, M.S. Khil, H.Y. Kim, I. Kim Soo, Mater. Sci. Eng. **28**, 70 (2008)
17. Y. Ishii, H. Sakai, H. Murata, Mater. Lett. **62**, 3370 (2008)
18. H. Tong, T. Okano, T. Iseki, T. Yano, J. Mater. Sci. **30**, 3087 (1995)
19. D. Dong, S. Tasaka, N. Inagaki, Polym. Degrad. Stab. **72**, 345 (2001)
20. K.Y. Park, S.E. Lee, C.G. Kim, J.H. Han, Compos. Struct. **81**, 401 (2007)
21. Y. Huang, N. Li, Y.F. Ma, F. Du, F.F. Li, X.B. He, X. Lin, H.J.Y.D. Gao, Chem. Carbon **45**, 1614 (2007)
22. Y. Ikuma, H. Bessho, Int. J. Hydrogen Energy **32**, 2689 (2007)
23. Y. Wang, A. Zhou, Z. Yang, Mater. Lett. **62**, 1930 (2008)
24. X. Chen, S.S. Mao, Chem. Rev. **107**, 2891 (2007)
25. S.J. O'Connor, K.J.D. MacKenzie, M.E. Smith, J.V. Hanna, J. Mater. Chem. **20**, 10234 (2010)
26. C. Wang, X.M. Zhang, X.F. Qian, Y. Xie, W.Z. Wang, Y.T. Qian, Mater. Res. Bull. **33**(12), 1747 (1998)
27. S. Zhu, D. Zhang, X. Zhang, L. Zhang, X. Ma, Y. Zhang, M. Cai, Micropor. Mesopor. Mater. **126**, 20 (2009)
28. L. Sun, J. Li, C. Wang, S. Li, Y. Lai, H. Chen, C. Lin, J. Hazard. Mater. **171**, 1045 (2009)
29. D. Yang, S.E. Park, J.K. Lee, S.W. Lee, J. Cryst. Growth **311**, 508 (2009)
30. S.W. Lee, S. Obregón-Alfaro, V. Rodríguez-González, J. Photochem. Photobiol. **221**, 71 (2011)
31. J. Guo, S. Zhu, Z. Chen, Y. Li, Z. Yu, J. Li, C. Feng, D. Zhang, Ultrasonics Sonochem. **18**, 1082 (2011)
32. P. Gibot, C. Vix-Guterl, J. Eur. Ceram. Soc. **27**, 2195 (2007)
33. V. Collins-Martinez, A.L. Ortiz, A.A. Elguezabal, Int. J. Chem. React. Eng. **5**, A92 (2007)
34. C.L. Luu, Q.T. Nguyen, S.T. Ho, Adv. Nat. Sci. **1**, 015008 (2010)
35. K. Wantala, L. Laokiat, P. Khemthong, N. Grisdanurak, K. Fukaya, J. Taiwan, Int. Chem. Eng. **41**, 612 (2010)
36. N. Serpone, D. Lawless, R. Khairutdinov, J. Phys. Chem. **99**, 16646 (1995)
37. E.M. Patterson, C.E. Shelden, B.H. Stockton, Appl. Opt. **16**, 729 (1977)
38. J.G. Yu, X.X. Yu, Environ. Sci. Technol. **42**, 4902 (2008)
39. B. Erdem, R.A. Hunsicker, G.W. Simmons, E.D. Sudol, V.L. Dimonie, M.S. El-Aasser, Langmuir **17**, 2664 (2001)
40. M.H. Zhou, J.G. Yu, B. Cheng, H.G. Yu, Mater. Chem. Phys. **93**, 159 (2005)
41. Y.Y. Wang, K. Kusumoto, C.J. Li, Phys. Procedia **32**, 95 (2012)
42. V. Keller, F. Garin, Catal. Commun. **4**, 377 (2003)
43. Y. Zhang, Y. Xu, T. Li, Y. Wang, Particuol **10**, 46 (2012)